J. Meas. Sci. Instrum., 2025, 16(2): 313-322. http://jmsi.publish.founderss.cn/
DOI: 10.62756/jmsi.1674-8042.2025030 jmsi@nuc.edu.cn

Four-wheel positioning homography matrix optimization algorithm based on minimum re-projection error

YAN Hongjie[1], ZHU Zhifeng[1*], CAI Bohua[2], YAO Yong[2]

1. School of Electrical and Information Engineering, Anhui University of Technology, Ma'anshan 243000, China;
2. Anhui FCAR Electronic Technology Co., Ltd., Ma'anshan 243000, China

***Corresponding author:** ZHU Zhifeng (zzf@ahut.edu.cn)

Received: March 5, 2024 **Revised:** April 13, 2024 **Accepted:** June 13, 2024

Abstract: A fast and accurate homography matrix method for four-wheel positioning detection was presented in the paper. Fewer sensors were required with simpler operation and faster detection. Firstly, eight feature points were extracted by using the target detection algorithm based on the fitting method. Secondly, six feature points were obtained by line fitting-based selection. Thirdly, from the selected six feature points, five points were randomly chosen to minimize the re-projection error. Finally, four points were randomly selected from these five feature points to find the homography matrix, and the other point was back to the homography matrix for verification. The experimental results show that the mean re-projection error is reduced by about 3.41%—4.57% compared with the modified RANSAC (Random sample consensus) algorithm. With the optimized algorithm, the error is reduced by about 12.81%—13.86% compared with the improved RANSAC algorithm. Compared with traditional targets, the average calibration time is reduced by about 26.95%—27.88%. The results indicated that the combination of target algorithm and optimization algorithm could ensure the accuracy and reliability of four-wheel positioning.

Key words: computer vision; four-wheel alignment; line fitting; re-projection error; homography matrix

0 Introduction

The safety and stability of the vehicle are greatly influenced by four-wheel positioning. According to the difference between measurement principle and measurement equipment, the traditional four-wheel positioner is roughly divided into four categories: mechanical positioner, laser positioner, CCD positioner, and 3D positioner[1]. Among them, the 3D positioner is the most popular in the current market because of its high positioning accuracy and convenient operation[2]. However, in the implementation of 3D four-wheel positioning, the optimization of the homography matrix becomes a key challenge[3]. The homography matrix is an algorithm used to connect the two-dimensional image captured by the camera to the three-dimensional world coordinates of the vehicle[4]. A variety of complexities need to be overcome in the optimization of its four-wheel positioning, with data noise being one of the main problems[5]. As one of the main obstacles of homography matrix optimization, data noise is caused by the image data captured by the camera, which usually contains various types of noise and distortion. Even small image noise may result in a significant impact on the estimation of the homography matrix, thereby affecting the accurate positioning of the vehicle. The noise can be either random, such as electronic noise or environmental conditions, or systematic, such as lens distortion or image transmission problems[6].

Xu et al.[7] proposed to construct the measurement and verification model of caster and kingpin inclination (KPI) through the size bridge, and achieved high measurement accuracy through fewer sizes and features. Li et al.[8] only needed to obtain two depth images and the coordinates of four three-dimensional feature points in each depth image to complete. For the two methods, although the data noise is reduced to a certain extent, too few feature points will inevitably be accidental. In addition, Perez et al.[9] used multi-camera and multi-image calibration. Although the obtained images are accurate, the camera position needs to be repeatedly modified to match the correct ratio, and the process is too cumbersome. In addition to reducing feature extraction to reduce data noise, Wei et al.[10] also reduced data noise by filtering image pixels, but it took a long time. The high-precision camera method based on sub-pixel edge detection and center correction compensation proposed by Kang et al. effectively improved the camera calibration

© The Author(s) 2025. Published by Publishing Center of North University of China. The articles published in this open access journal are distributed under the terms of the Creative Commons Attribution 4.0 International License (http://creativecommons.org/licenses/by/4.0/), which permits use, distribution and reproduction in any medium, provided the original work is properly cited.

accuracy[11].

A 3D four-wheel positioning single camera calibration method was designed in this paper, which utilized a single target to calibrate the camera parameters with high precision and speed, and optimized the key parameters to reduce the data acquisition error and improve the detection speed. Firstly, by applying vector detection and three-dimensional perspective theory, the equation for solving the homography matrix was established. Then, a special circular pattern target was designed, and more accurate feature points were selected by fitting the linear sieve. Finally, the minimum re-projection error was introduced to filter out the optimal homography matrix. In order to ensure that the re-projection error corresponding to the calculated homography matrix was the smallest, comparative experiments and real vehicle tests were carried out with the improved RANSAC algorithm.

1 System model

1.1 Camera calibration coordinate system

In order to more accurately describe the relationship between the pixels on the image and the spatial three-dimensional points during the camera calibration process, four different coordinate systems are usually defined, as shown in Fig. 1, including the world coordinate system $(O_w - X_w Y_w Z_w)$, the camera coordinate system $(O_c - X_c Y_c Z_c)$, the image plane coordinate system $(O' - XY)$, and the pixel coordinate system $(O - UV)$[12].

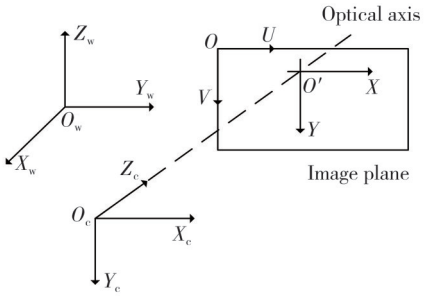

Fig. 1 Four coordinate systems of camera calibration

These four coordinate systems are interrelated[13]. Firstly, in the process of camera calibration and camera pose estimation, it is necessary to convert the three-dimensional points in the world coordinate system to the camera coordinate system. This process can be realized by rigid body transformation, that is, it can be expressed by rotation matrix and translation matrix[14]. Then, the camera coordinates are projected onto the image plane coordinates through perspective projection. Finally, the image plane coordinates are converted twice pixel coordinates. Among them, the secondary transformation refers to the process of mapping the coordinate values in the image plane coordinate system to the pixel coordinate system[15].

Ideally, the imaging process of the camera can be described by a linear pinhole imaging model, which simplifies the complexity of the camera imaging process and allows us to use a relatively simple set of parameters to describe the imaging characteristics of the camera[16,17].

$$s\begin{bmatrix} U \\ V \\ 1 \end{bmatrix} = \begin{bmatrix} \frac{1}{\mathrm{d}X} & 0 & u_0 \\ 0 & \frac{1}{\mathrm{d}Y} & v_0 \\ 0 & 0 & 1 \end{bmatrix} \begin{bmatrix} f & 0 & 0 & 0 \\ 0 & f & 0 & 0 \\ 0 & 0 & 1 & 0 \end{bmatrix} \begin{bmatrix} \boldsymbol{R} & \boldsymbol{t} \\ 0 & 1 \end{bmatrix} \begin{bmatrix} X_w \\ Y_w \\ Z_w \\ 1 \end{bmatrix} =$$

$$\begin{bmatrix} f_x & 0 & u_0 & 0 \\ 0 & f_y & v_0 & 0 \\ 0 & 0 & 1 & 0 \end{bmatrix} \begin{bmatrix} \boldsymbol{R} & \boldsymbol{t} \\ 0 & 1 \end{bmatrix} \begin{bmatrix} X_w \\ Y_w \\ Z_w \\ 1 \end{bmatrix} = \boldsymbol{K}\boldsymbol{T} \begin{bmatrix} X_w \\ Y_w \\ Z_w \\ 1 \end{bmatrix}, \quad (1)$$

where s is a non-zero scale factor; $\frac{1}{\mathrm{d}X}$ represents the reciprocal of the actual physical size of each pixel in the horizontal direction of the image; $\frac{1}{\mathrm{d}Y}$ represents the reciprocal of the actual physical size of each pixel in the vertical direction of the image; f is the focal length; f_x and f_y are the normalized camera focal lengths along the X and Y axes, respectively; $\boldsymbol{R}$ is the rotation matrix; $\boldsymbol{t}$ is the translation matrix; (u_0, v_0) is the translated origin coordinates; $\boldsymbol{K}$ is the camera intrinsic parameter matrix; $\boldsymbol{T}$ is the camera extrinsic parameter matrix.

1.2 Calculation of intrinsic parameter matrix

The intrinsic parameter matrix is one of the most important parameters in camera calibration. It is described by the internal imaging characteristics of the camera, including the focal length, imaging center, pixel size, and other information about the camera. Setting an accurate internal parameter matrix can lead to higher accuracy and precision in the imaging process of the camera, thereby improving the effectiveness of camera vision applications[18].

Suppose that the three-dimensional coordinate (x_c, y_c, z_c) in the camera coordinate system and the two-dimensional coordinate (x, y) in the image coordinate system are substituted into the Eq. (2) to obtain the internal parameter matrix $\boldsymbol{A}$. Because $\boldsymbol{A}$ contains four unknowns, two sets of three-dimensional coordinates and two-dimensional coordinates are needed.

$$\begin{cases} x = (x_c / z_c) f_x + u_0, \\ y = (y_c / z_c) f_y + v_0, \end{cases} \quad (2)$$

$$A=\begin{bmatrix} f_x & 0 & u_0 \\ 0 & f_y & v_0 \\ 0 & 0 & 1 \end{bmatrix}. \tag{3}$$

1.3 Calculation of homography matrix

After obtaining the two-dimensional image coordinates and three-dimensional spatial coordinates, for ease of computation, it is common practice to align the world coordinate system with the plane inside the target, and make them parallel to the image plane. This is denoted as $Z_w=0$. All the points in the above equation can be written in the form of homogeneous coordinates. When the points are written in the form of homogeneous coordinates, it can be realized by adding an element 1 at the end of the original coordinate vector, and the three-dimensional coordinates are normalized to obtain

$$s\begin{bmatrix} U \\ V \\ 1 \end{bmatrix}=\begin{bmatrix} f_x & 0 & u_0 \\ 0 & f_y & v_0 \\ 0 & 0 & 1 \end{bmatrix}\begin{bmatrix} \boldsymbol{R}_1 & \boldsymbol{R}_2 & \boldsymbol{t} \end{bmatrix}\begin{bmatrix} X_w \\ Y_w \\ 1 \end{bmatrix}= A\begin{bmatrix} \boldsymbol{R}_1 & \boldsymbol{R}_2 & \boldsymbol{t} \end{bmatrix}\begin{bmatrix} X_w \\ Y_w \\ 1 \end{bmatrix}, \tag{4}$$

where $\boldsymbol{R}_1$ and $\boldsymbol{R}_2$ represent the first two columns of the rotation matrix $\boldsymbol{R}$.

Let the homography matrix $\boldsymbol{H}$ be the product of the intrinsic and extrinsic parameter matrices, forming the perspective projection matrix.

$$\boldsymbol{H}=\begin{bmatrix} \boldsymbol{H}_1 & \boldsymbol{H}_2 & \boldsymbol{H}_3 \end{bmatrix}=\begin{bmatrix} H_{11} & H_{12} & H_{13} \\ H_{21} & H_{22} & H_{23} \\ H_{31} & H_{32} & H_{33} \end{bmatrix}= A\begin{bmatrix} \boldsymbol{R}_1 & \boldsymbol{R}_2 & \boldsymbol{t} \end{bmatrix}. \tag{5}$$

Based on the mapping relationship between the image coordinate system and the world coordinate system, there is

$$s\begin{bmatrix} U \\ V \\ 1 \end{bmatrix}=\begin{bmatrix} H_{11} & H_{12} & H_{13} \\ H_{21} & H_{22} & H_{23} \\ H_{31} & H_{32} & H_{33} \end{bmatrix}\begin{bmatrix} X_w \\ Y_w \\ 1 \end{bmatrix}. \tag{6}$$

Let (x_i,y_i) represent the three-dimensional coordinates in space, and (x_i',y_i') represent the two-dimensional coordinates on the image plane. Each feature point corresponds to two homography equations, and then there are $2n$ equations for n feature points.

$$\begin{bmatrix} -x_1 & -y_1 & -1 & 0 & 0 & 0 & x_1x_1' & x_1'y_1 & x_1' \\ 0 & 0 & 0 & -x_1 & -y_1 & -1 & x_1y_1' & y_1'y_1 & y_1' \\ -x_2 & -y_2 & -1 & 0 & 0 & 0 & x_2x_2' & x_2'y_2 & x_2' \\ 0 & 0 & 0 & -x_2 & -y_2 & -1 & x_2y_2' & y_2'y_2 & y_2' \\ \vdots & \vdots & \vdots & \vdots & \vdots & \vdots & \vdots & \vdots & \vdots \\ -x_n & -y_n & -1 & 0 & 0 & 0 & x_nx_n' & x_n'y_n & x_n' \\ 0 & 0 & 0 & -x_n & -y_n & -1 & x_ny_n' & y_n'y_n & y_n' \end{bmatrix}\begin{bmatrix} H_{11} \\ H_{12} \\ H_{13} \\ H_{21} \\ H_{22} \\ H_{23} \\ H_{31} \\ H_{32} \\ H_{33} \end{bmatrix}=\begin{bmatrix} 0 \\ 0 \\ 0 \\ 0 \\ 0 \\ 0 \\ 0 \\ 0 \\ 0 \end{bmatrix}. \tag{7}$$

1.4 Calibration board and fitting algorithm

There are many target circles on the traditional calibration board and the distribution is uniform and regular, resulting in more feature points that can be selected, which makes the calculation redundancy larger, and the selection of feature points is more random, which is easy to cause large errors, as shown in Fig.2.

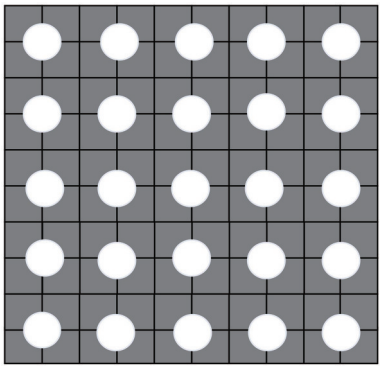

Fig. 2 Traditional calibration board

Four feature points are needed to solve a homography matrix. The calibration plate of the fitting algorithm is adopted, wherein the rectangular target is preferred over the square target to divide the space into left and right parts, and the target circles are symmetrically and dispersal marked on the target. This approach reduces the randomness in the selection of feature points, minimizing the potential for large errors caused by excessive calculation redundancy and random feature point selection. The center of each target circle can be quickly distinguished and marked by ellipse fitting, so as to improve the efficiency of finding the target circle and the center of the circle. In addition, in the optimization process of the homography matrix, two sample points are randomly selected to fit the straight line, and the abnormal points or noise points can be excluded. Abnormal points may be caused by measurement error, image noise, or other factors, which may have adverse effects on subsequent analysis or application. By fitting

straight lines and excluding outliers, more accurate and reliable results can be obtained. Although there are four-point collinear cases, because an additional set of feature points is added to verify the singularity matrix, the situation will not affect the final result. After the above conditions are excluded, there are only two points of the remaining fitted lines that are collinear, as shown in Fig.3.

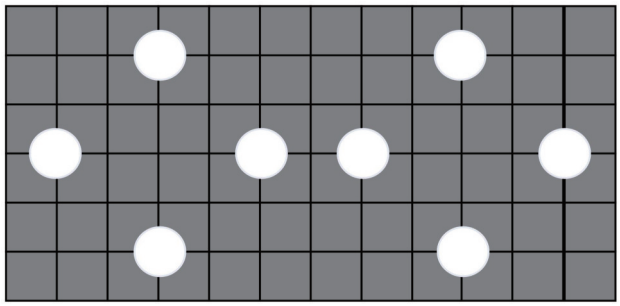

Fig. 3 Calibration board and fitting algorithm

1.5 Optimization of homography matrix

Two sample points are randomly selected from the extracted feature points to fit the straight line, and the internal and external points are distinguished by setting the threshold. A predefined threshold is exceeded by the number of interior points, and the interior point set is obtained by repeating the process until a certain number of iterations is reached. Then, for the extracted feature points, the average re-projection error is calculated as the constraint condition. From the interior point set, five sets of feature points are randomly selected to calculate the re-projection error. If it is less than the average re-projection error, the constraint condition is updated until the re-projection error is less than the set threshold and the re-projection error change is less than the set threshold. After screening out five groups of feature points, four groups are randomly selected to calculate the homography matrix, and the remaining group is substituted back to the homography matrix. The optimal homography matrix is obtained when the distance between the obtained coordinates and the actual coordinates falls within the set range, and the optimization of the homography matrix is completed.

The re-projection error among them refers to the information loss caused by projecting the data from a high-dimensional space to a low-dimensional space. In the process of dimensionality reduction, some characteristics, changes, or structures of the original data may not be completely preserved in the low-dimensional projection, which may lead to the loss of some useful information in the data after dimensionality reduction. Some useful information in the data may be lost when the data is projected from high-dimensional space to low-dimensional space, depending on the size of the re-projection error. Preserving as much information and the structure of the original data as possible in the low-dimensional space is often regarded as an advantage in the dimensionality reduction process, where the smaller projection error representation leads to less information being lost[19].

2 Solution for optimal homography matrix

2.1 Filtering feature points

Although 8 two-dimensional coordinate points are selected by collecting the target of the fitting algorithm, in order to ensure the accuracy and speed of the results, the feature points are continuously selected from these 8 feature points, and the selected feature points are placed in the interior point set. Two sample points are randomly selected from the eight feature points as (a_1, b_1), (a_2, b_2), and the fitting line $y = Mx + c$ is obtained. M represents the slope and c represents the constant.

The distance from the remaining feature point of the fitting line is recorded as $l_i (i = 3, 4, \cdots, 8)$, and the distance threshold L is set. When the distance from the remaining feature point of the fitting line is less than the set distance threshold, that is, $l_i < L$, and the point is saved to the interior point set[20]. Each time, the number of iterations is added to 1, and the above process is repeated until the number of interior points is greater than or equal to the set interior point threshold N and the number of iterations is greater than k. The distance formula from the remaining feature points to the fitting line is

$$l_i = \frac{|Ma_i - b_i + c|}{\sqrt{M^2 + 1}} (i = 3, 4, \cdots, 8). \tag{8}$$

2.2 Setting number of iterations

The number of iterations, k, can be computed by using RANSAC[21,22]. The formula is

$$k = \log_{(1-(1-\varepsilon)^m)}(1 - p), \tag{9}$$

where confidence level p is expressed with percentage, representing the probability of obtaining the best-fitting model after k iterations, ε denotes the outlier ratio of the total sample, and m represents the minimum number of sample points required to compute a homography matrix model. There are common confidence levels of 90%, 95%, 98%, and 99%. The precision of the estimate

may be limited by potentially widening the confidence interval, which implies that greater confidence levels but may be caused by higher confidence. Therefore, a confidence level of $p = 0.995$ is chosen. When the threshold number N of the interior point is 5 and substituted into Eq. (9), the calculated iteration number k is larger. And when N is 6, the calculated iteration number k is significantly less. Therefore, if N is 6, the number of iterations is less and the speed is faster.

2.3 Setting distance threshold

The distance from the remaining feature points of the fitted line is denoted as $l_i (i = 3,4,\cdots,8)$, and their mean μ and standard deviation σ are calculated by

$$\mu = \frac{(l_3 + l_4 + \cdots + l_8)}{6}, \tag{10}$$

$$\sigma = \frac{\sqrt{(l_3 - \mu)^2 + (l_4 - \mu)^2 + \cdots + (l_8 - \mu)^2}}{6}. \tag{11}$$

An appropriate threshold multiple k_L is chosen to multiply the standard deviation to get the threshold size. 1 times, 2 times, or 3 times the standard deviation are often chosen.

$$L = k_L \sigma. \tag{12}$$

It is understood that a total of 6 feature points needs to be selected. Since 2 sample points are already available, an additional 4 feature points need to be selected to ensure that 4 feature points are chosen. Therefore, to ensure the selection of 4 feature points, the threshold multiplier $k_L = 2$ is set. In this way, the distance threshold L is obtained.

2.4 Establishing constraint conditions

For a target that fits the matching algorithm, eight two-dimensional coordinate points are selected. The average re-projection error of these points is computed to serve as the initial constraint for a secondary screening of the inlier set. The relationship between the camera and the re-projection error is mainly affected by the internal and external parameters of the camera, the size and distribution of the target on the image, and the distance between the target and the camera. And the target distance is one of the relation between the camera and the re-projection error.

Assuming a three-dimensional coordinate $P = \{(x_{c1}, y_{c1}, z_{c1}), (x_{c2}, y_{c2}, z_{c2}), \cdots, (x_{cn}, y_{cn}, z_{cn}\}$ in the camera coordinate system, its corresponding pixel coordinates can be represented as $Q = \{(x_1, y_1), (x_2, y_2), \cdots, (x_n, y_n)\}$. Each three-dimensional point P_i is projected onto the image plane, resulting in a projected point $P_i' = (u_i, v_i)$. The Euclidean distance d_i between each projected point P_i' and its corresponding two-dimensional feature point Q_i is calculated. Then, the sum of all the Euclidean distances of the projected points is computed as D. Finally, the obtained average error is computed as the re-projection error E_{ave}.

$$d_i = \sqrt{(u_i - x_i)^2 + (v_i - y_i)^2}, \tag{13}$$

$$D = d_1 + d_2 + \cdots + d_n, \tag{14}$$

$$E_{ave} = \frac{D}{n}. \tag{15}$$

Five groups of feature points are randomly selected as the interior point set, and the re-projection error is calculated using the method mentioned earlier. Assuming that the re-projection error is E_1, it is compared with the average re-projection error E_{ave}. If it is less than E_{ave}, the update constraint is E_1, otherwise re-select the point.

2.5 Minimum re-projection error

When the restriction is no longer E_{ave}, assume that the restriction is updated to E_1. Five sets of feature points are randomly selected from the set of interior points, and the re-projection error is calculated. It is assumed that E_2 is compared with E_1. If $E_2 > E_1$, then go back to the interior point set to re-select points; and if $E_2 < E_1$, then update the constraint to E_2.

The re-projection error obtained each time is compared with the re-projection error obtained last time, and the two errors are subtracted, and the absolute value of the difference is less than the convergence threshold ΔE_{set}, that is, $|E_2 - E_1| < \Delta E_{set}$. The re-projection error E_2 obtained at this time is the minimum re-projection error E_{min}.

The formula for the convergence threshold is

$$\Delta E_{set} = \frac{|E_2 - E_1|}{E_2}, \tag{16}$$

where E_1 is the re-projection error used as the constraint in the previous iteration, and E_2 is the current re-projection error used as the constraint.

2.6 Optimal homography matrix

The minimum re-projection error E_{min} is calculated, and five sets of feature points are obtained accordingly. Because the homography matrix contains nine unknown, and one feature point corresponds to two equations, four sets of feature points are randomly selected from the five sets of feature points and substituted into Eq. (7), and an additional equation $H_{31} x_i + H_{32} y_i + H_{33} = 1$ is added to

solve the homography matrix. The remaining set of feature points is substituted back to the solved homography matrix to calculate the three-dimensional coordinates in the space. Comparing the solved three-dimensional coordinates with the actual three-dimensional coordinates, if the distance between the two points is less than the set nearest distance r_{set}, the matrix is verified to be the optimal homography matrix. The nearest distance threshold is the result obtained by many experiments, and $r_{set}=0.015$ cm is set. If the distance between the two points is greater than the set nearest distance, it returns to 2.1.

The process of solving the optimal homography matrix as described can be displayed in Fig.4.

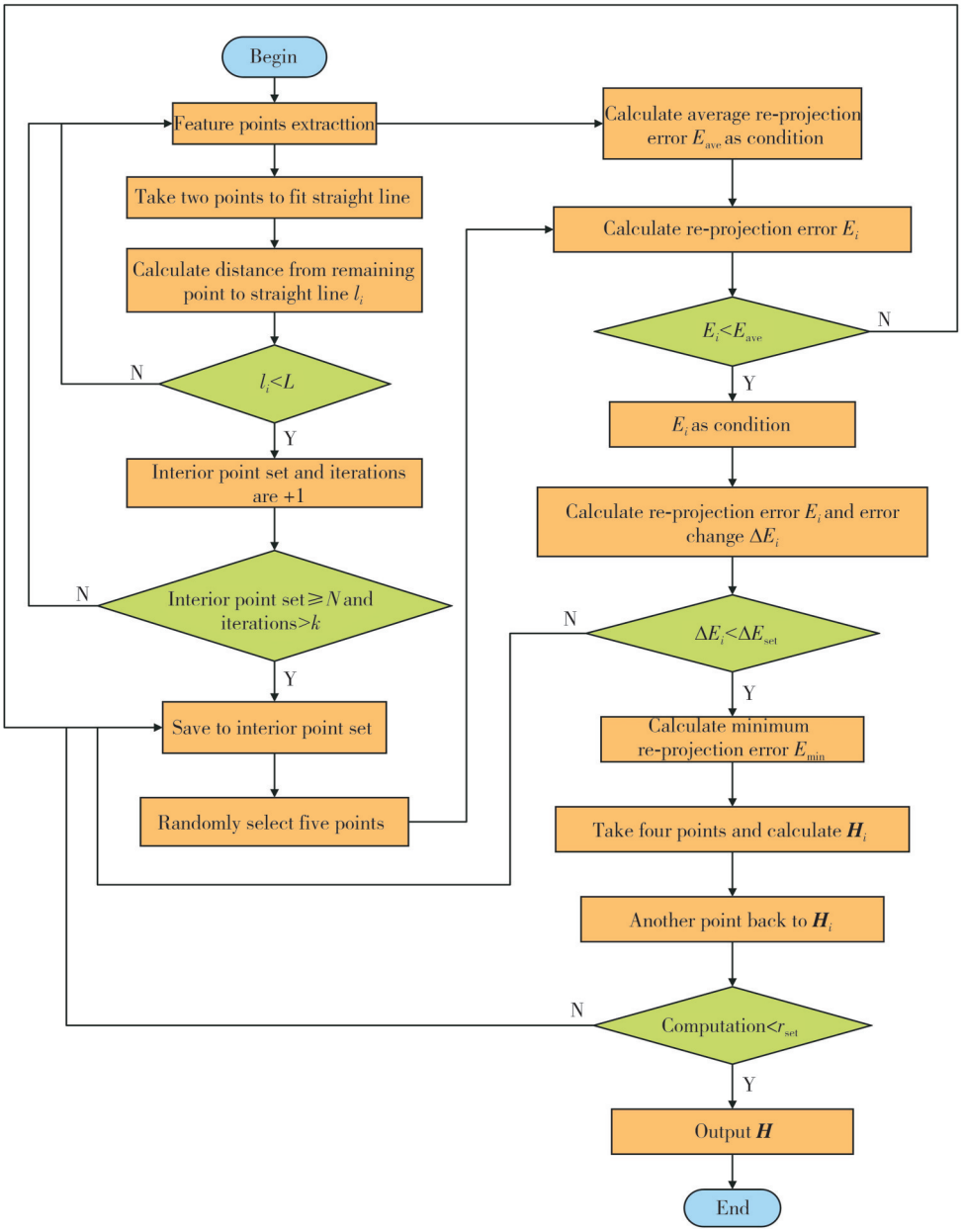

Fig. 4 Calculate homography matrix *H* flow chart

3 Experiment

3.1 Optimal homography matrix test

In this experiment, the principle of monocular camera calibration was adopted. The industrial camera of model M2S500M-H2 was used to fix the industrial camera. The target was placed 2 m away from the camera. After each image was taken, the target was moved with a displacement of 0.2 m in order to simulate the slow operation of the car during the calibration process. The target plate uses the traditional target and the target of the fitting algorithm, and takes ten photos of each of the two targets.

Fig. 5 is fit algorithm target images, and Fig. 6 is traditional target image. After the screening of the fitted

straight line and the minimum re-projection error, and the verification of the homography matrix by the feature point back substitution, the final calculated homography matrix was the optimal homography matrix.

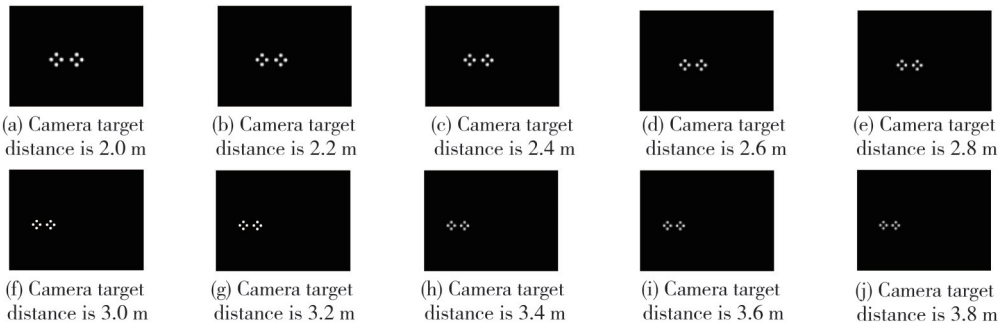

(a) Camera target distance is 2.0 m (b) Camera target distance is 2.2 m (c) Camera target distance is 2.4 m (d) Camera target distance is 2.6 m (e) Camera target distance is 2.8 m

(f) Camera target distance is 3.0 m (g) Camera target distance is 3.2 m (h) Camera target distance is 3.4 m (i) Camera target distance is 3.6 m (j) Camera target distance is 3.8 m

Fig. 5 Fit algorithm target images

When the homography matrix optimization method was applied to the traditional target and the matching algorithm target, respectively, the parameters such as internal parameter matrix, homography matrix, and calibration time were obtained. The optimization effect was determined by the re-projection error. The traditional target optimal results are shown in Table 1, and the matching algorithm target optimal results are shown in Table 2. "Before optimization" referred to the improved RANSAC algorithm, and "after optimization" referred to the algorithm proposed in the paper.

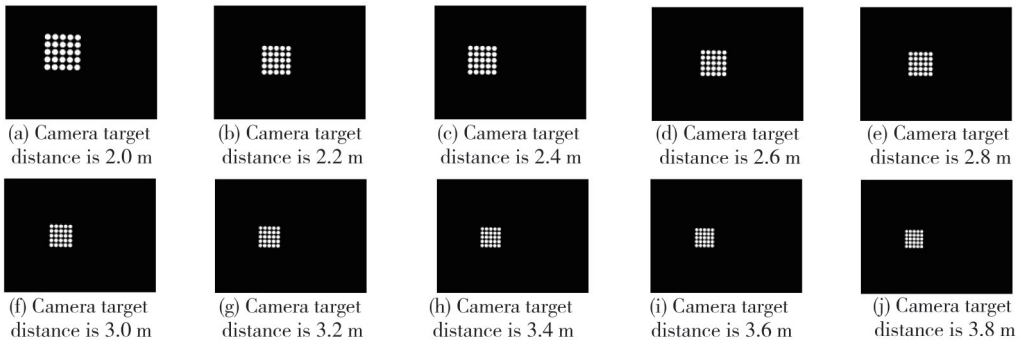

(a) Camera target distance is 2.0 m (b) Camera target distance is 2.2 m (c) Camera target distance is 2.4 m (d) Camera target distance is 2.6 m (e) Camera target distance is 2.8 m

(f) Camera target distance is 3.0 m (g) Camera target distance is 3.2 m (h) Camera target distance is 3.4 m (i) Camera target distance is 3.6 m (j) Camera target distance is 3.8 m

Fig. 6 Traditional target images

Table 1 Optimization results of traditional target

Stage	Intrinsic matrix	Homography matrix	Average re-eprojection error/pixel	Average calibration time/s
Before optimization	$\begin{bmatrix} 2\,097.427 & 0 & 637.539 \\ 0 & 2\,792.845 & 530.510 \\ 0 & 0 & 1 \end{bmatrix}$	$\begin{bmatrix} 0.023\,63 & -0.010\,47 & -6.425\,63 \\ -0.003\,92 & 0.009\,79 & -3.815\,72 \\ 0.000\,21 & -0.002\,43 & 1 \end{bmatrix}$	0.254 299	3.385 19
After optimization	$\begin{bmatrix} 2\,098.621 & 0 & 673.952 \\ 0 & 2\,793.728 & 531.381 \\ 0 & 0 & 1 \end{bmatrix}$	$\begin{bmatrix} 0.00015 & -0.007\,83 & 3.995\,90 \\ 0.00031 & -0.015\,69 & 8.006\,00 \\ 0.00038 & -0.001\,96 & 1 \end{bmatrix}$	0.219 056	3.195 86

Table 2 Fits target optimization results of algorithm

Stage	Intrinsic matrix	Homography matrix	Average re-projection error/pixel	Average calibration time/s
Before optimization	$\begin{bmatrix} 2\,115.059 & 0 & 682.105 \\ 0 & 2\,820.079 & 511.579 \\ 0 & 0 & 1 \end{bmatrix}$	$\begin{bmatrix} 0.038\,06 & -0.073\,02 & 4.070\,98 \\ 0.100\,92 & -0.067\,05 & 2.419\,52 \\ 0.008\,80 & -0.003\,58 & 1 \end{bmatrix}$	0.263 270	4.634 12
After optimization	$\begin{bmatrix} 2\,114.171 & 0 & 682.121 \\ 0 & 2\,816.771 & 511.617 \\ 0 & 0 & 1 \end{bmatrix}$	$\begin{bmatrix} 0.077\,48 & -0.049\,79 & 11.387\,60 \\ 0.011\,56 & -0.023\,13 & 9.331\,46 \\ 0.003\,97 & -0.003\,46 & 1 \end{bmatrix}$	0.229 548	4.431 45

The average re-projection error in the experimental data is analyzed, as shown in Fig.7. It can be seen that the average re-projection error using the conjunction algorithm target is smaller than the average re-projection

error using the traditional target. Combined with the quantitative analysis of the experimental data, the average re-projection error on the target using the fit algorithm before the algorithm optimization is reduced by 3.41%, and the average re-projection error of the target using the fit algorithm after the algorithm optimization is reduced by 4.57%. After the algorithm is optimized, the re-projection error is also reduced accordingly. Combined with the quantitative analysis of the experimental data, for the traditional target, the average re-projection after the optimization algorithm is reduced by 12.81%. For the target of the fit algorithm, the average re-projection after the optimization algorithm is reduced by 13.86%.

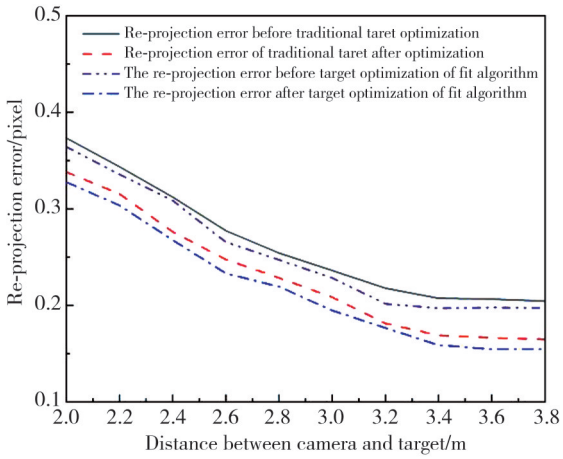

Fig. 7 Comparison of re-projection error

The average calibration time in the experimental data is analyzed, as shown in Fig.8.

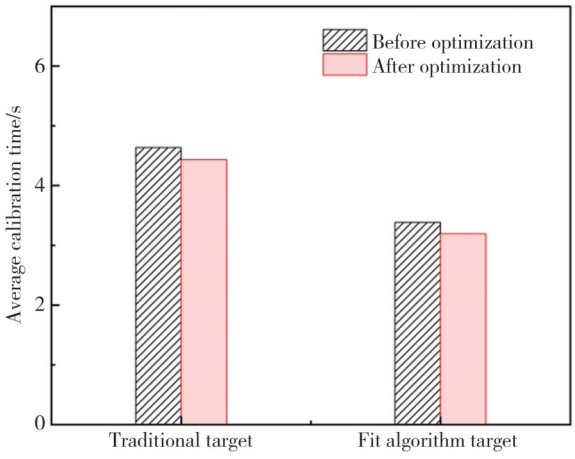

Fig. 8 Comparison of calibration time

It can be seen that the average calibration time using the fitting algorithm target is shorter than the average calibration time using the traditional target. Combined with the quantitative analysis of experimental data, the average calibration time efficiency of using the fit algorithm before the algorithm optimization is increased by 26.95%, and the average calibration time efficiency of using the fit algorithm after the algorithm optimization is increased by 27.88%. After the algorithm was optimized, the average calibration time was also shortened. Combined with the quantitative analysis of experimental data, for the traditional target, the average calibration time efficiency is improved by 4.37% after using the optimization algorithm. For the matching algorithm target, the average calibration time efficiency over using the optimization algorithm is increased by 5.59%.

3.2 Real vehicle test

In the real vehicle test, the selected model was a Skoda car, and the target of the fit algorithm was fixed on the wheel hub by using the fixture. The camera was an industrial camera with 5 million pixels, which moved the vehicle and took pictures with the camera. In order to avoid the problem of experimental data error caused by too few experiments, the car was tested ten times. After each experiment, the vehicle moved a certain distance. When the test vehicle was placed at different distances, whether the target using the fitting algorithm affected the collection of the target plate, thus influencing the accuracy of the calibration.

The standard data of the automobile manufacturer is shown in Table 3, while the real vehicle test results are shown in Table 4.

Table 3 Standard data of automobile manufacturers

Standard data	Camber	Toe
Standard minimum value	−1°14′	−0°07′
Standard maximum value	−0°14′	0°07′

Table 4 Real vehicle test results data

Distance between camera and target/m	Camber	Toe
2.0	−0°12′	0°05′
2.2	−0°10′	0°05′
2.4	−0°19′	0°04′
2.6	−0°18′	0°04′
2.8	−0°18′	0°03′
3.0	−0°18′	0°03′
3.2	−0°16′	0°02′
3.4	−0°16′	0°02′
3.6	−0°16′	0°02′
3.8	−0°16′	0°02′

Comparison curves between the real vehicle test results and the standard data of the automobile manufacturer are shown in Fig.9.

Comparing Table 3 and Table 4, it can be seen that when the vehicle is within the range of 2 m—3.8 m from the calibration device, the parameters of the ten experimental results are basically consistent and within

the error range. The reliability of the four-wheel alignment detection using the calibration target plate was verified, and the effectiveness of the detection device and optimization algorithm designed in the paper was also verified.

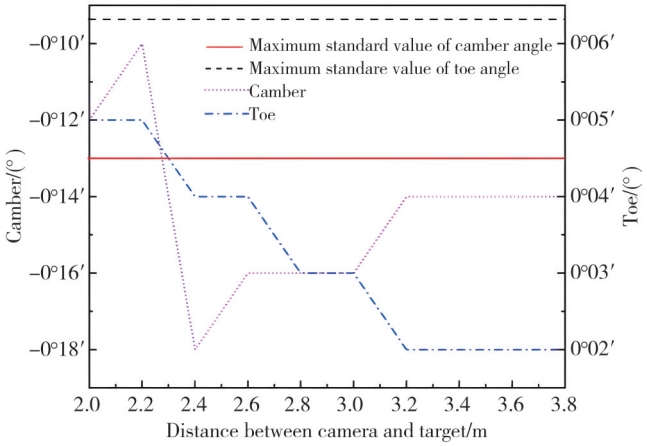

Fig. 9 Comparison curves of real vehicle test results and standard data of automobile manufacturers

4 Conclusions

The computer vision theory was used to investigate the method of solving four-wheel alignment parameters and optimizing the homography matrix.

By matching the target of the algorithm, eight most representative feature points were selected, and the average re-projection error calculated was significantly reduced before and after the algorithm optimization, respectively. This showed that the fitting algorithm target had better accuracy and stability in the calibration process. For the traditional target and the fit algorithm target, significant error reduction could be brought by the optimization algorithm, respectively. It showed that the feature point screening method using the conjunction algorithm could effectively capture the feature points related to the four-wheel positioning, thus providing more accurate and efficient data for subsequent calculations.

The method of fitting straight lines was used to minimize the re-projection error. Then the homography matrix was verified by the remaining point back substitution. Before and after the optimization of the algorithm, the average calibration time efficiency of the target of the fit algorithm was increased, respectively, while in the case of traditional target, the average calibration time efficiency over using the optimization algorithm was increased, respectively. This meant that through the optimization algorithm, the time required in the calibration process could be significantly reduced and the calibration efficiency could be improved.

Combined with the above optimization process, according to the field test data, in the range of 2 m—3.8 m of the vehicle distance calibration device, it could well meet the requirements of four-wheel alignment detection. This proved the feasibility of using the target and optimization algorithm for four-wheel positioning. The traditional detection method was differentiated from by the utilization of computer vision theory and optimization technology, resulting in a significant enhancement in calibration efficiency and accuracy.

Acknowledgement

This work was supported by Anhui Province Key Research and Development Program (No. 2022107020012); Shenzhen Science and Technology Innovation Project (No. JSGG20191129102008260).

Declaration of conflicting interests

The authors have no conflict of interests related to this publication.

References

[1] SUN F. Research on uncertainty and calibration technology of automobile four-wheel positioning parameters. Zhenjiang: Jiangsu University, 2019.

[2] SHAO C H, ZHANG Z Y, XU S S, et al. Calibration point distribution study of a four-wheel alignment optimization device based on a blanket technology algorithm. Review of Scientific Instruments, 2020, 91(4): 044102.

[3] YANG W W, HE J L, LIU Q P, et al. Study on testing mechanism and experimental research of four-wheel alignment verification device. Metrology Science and Technology, 2022, 66(6): 54-59.

[4] PAN M Y, CHEN S W, LÜ X Y, et al. Error analysis on parameters measurement model of wheel-mounted four-wheel alignment//2020 11th International Conference on Prognostics and System Health Management, October 23-25, 2020, Ji'nan, China. New York: IEEE, 2020: 592-598.

[5] CHEN H, WANG D Q, CHEN Y Q. Research on the influence of calibration image on reprojection error//2021 International Conference on Big Data Engineering and Education, August 12-14, 2021, Guiyang, China. New York: IEEE, 2021: 60-66.

[6] ZHANG Z, ZHAO R J, LIU E H, et al. A single-image linear calibration method for camera. Measurement, 2018, 130: 298-305.

[7] XU G, HE W, CHEN F, et al. One-dimension orientation method of caster and kingpin inclination of vehicle wheel alignment. Measurement, 2022, 198: 111371.

[8] LI D D, CHEN G Z, LI C J, et al. 3D feature points

calibration method for depth-camera//2021 5th Asian Conference on Artificial Intelligence Technology, October 29-31, 2021, Haikou, China. New York: IEEE, 2021: 735-741.
[9] PEREZ A J, PEREZ-CORTES J C, GUARDIOLA J L. Simple and precise multi-view camera calibration for 3D reconstruction. Computers in Industry, 2020, 123: 103256.
[10] CHENG W, ZHU Z F, YAO Y, et al. An improved RANSAC algorithm for 3D wheel alignment. Journal of Measurement Science and Instrumentation, 2022, 13(4): 407-417.
[11] KANG C H, HONG L, REN J W, et al. High-precision camera calibration method based on sub-pixel edge detection and circularity correction compensation. Laser & Optoelectronics Progress, 2024, 61(8): 146-154.
[12] REN Y Z, HU F. Camera calibration with pose guidance// ICASSP 2021 - 2021 IEEE International Conference on Acoustics, Speech and Signal Processing, June 6-11, 2021, Toronto, ON, Canada. New York: IEEE, 2021: 2180-2184.
[13] YAO Y N, HUANG X Y, LÜ J L. A Space Joint calibration method for lidar and camera on self-driving car and its experimental verification//2021 6th International Symposium on Computer and Information Processing Technology, June 11-13, 2021, Changsha, China. New York: IEEE, 2021: 388-394.
[14] SUN W, HUO J, LI Y, et al. Combined calibration method for large field of view multi-camera system//2022 China Automation Congress, November 25-27, 2022, Xiamen, China. New York: IEEE, 2022: 4165-4170.
[15] HUANG C W, PAN X, CHENG J C, et al. Deep image registration with depth-aware homography estimation. IEEE Signal Processing Letters, 2023, 30: 6-10.
[16] JIANG P P. Research on fast calibration method of vehicle multi-camera vision system. Chongqing: Chongqing University of Posts and Telecommunications, 2020.
[17] XIN R, WU S H, LI A J. High-precision camera calibration method based on circular mode plane target. Journal of Yantai University: Natural Science and Engineering, 2020, 33(4): 472-478.
[18] SU F, WANG Z J. Error analysis and correction of a photoelastic method based on a pixelated polarization camera. Optics and Lasers in Engineering, 2023, 161: 107374.
[19] LI Z X, WANG K Q, JIA W Y, et al. Multiview stereo and silhouette fusion *via* minimizing generalized reprojection error. Image and Vision Computing, 2015, 33: 1-14.
[20] CHEN T, GUO J F, XIE X L, et al. High-precision image mosaic algorithm based on adaptive homography transform//2021 40th Chinese Control Conference, July 26-28, 2021, Shanghai, China. New York: IEEE, 2021: 3030-3035.
[21] ZENG D H. Research on image stitching technology based on partition detection and improved RANSAC algorithm. Chongqing: Southwest University, 2021.
[22] LIAN Z W, LIU Y, ZHANG Q. Research on algorithm of center positioning for automatic refractometer target ring. Journal of North University of China (Natural Science Edition), 2022, 43(6): 548-553.

基于最小重投影误差的四轮定位单应性矩阵优化算法

颜洪杰[1], 朱志峰[1*], 蔡伯华[2], 姚 勇[2]

1. 安徽工业大学 电气与信息工程学院, 安徽 马鞍山 243000;
2. 安徽省爱夫卡电子科技有限公司, 安徽 马鞍山 243000

摘 要: 本文提出了一种快速而准确的四轮定位检测方法, 具有传感器数量少、操作简单和检测速度快等特点。首先, 采用契合算法的标靶提取到8个特征点, 然后, 通过拟合直线进行筛选得到6个特征点。接着, 在筛选出的6个特征点中随机筛选出5个点, 使得求出的重投影误差最小。最后, 在这5个特征点中随机筛选4个点求单应性矩阵, 另一点回代单应性矩阵进行验证。实验结果显示, 采用契合算法标靶后, 平均重投影误差比改进的RANSAC算法降低约3.41%－4.57%; 采用优化算法后, 平均重投影误差比改进的RANSAC算法降低约12.81%－13.86%。与传统标靶相比, 平均标定时间减少约26.95%－27.88%。同时, 通过实车测试证明: 采用契合算法的标靶与优化算法结合可保证四轮定位的准确性和可靠性。

关键词: 计算机视觉; 四轮定位; 拟合直线; 重投影误差; 单应性矩阵

引用格式: YAN Hongjie, ZHU Zhifeng, CAI Bohua, et al. Four-wheel positioning homography matrix optimization algorithm based on minimum re-projection error. Journal of Measurement Science and Instrumentation, 2025, 16(2): 313-322. DOI: 10.62756/jmsi.1674-8042.2025030